International Journal of Applied Glass Science 3 [4] 349–368 (2012)
DOI:10.1111/ijag.12007

INTERNATIONAL JOURNAL OF
Applied Glass
SCIENCE

Multimaterial Fibers

Guangming Tao and Ayman F. Abouraddy*

CREOL, The College of Optics & Photonics, University of Central Florida, Orlando, Florida 32816

Alexander M. Stolyarov

Research Laboratory of Electronics, Massachusetts Institute of Technology, Cambridge, Massachusetts 02139

Recent progress in combining multiple materials with disparate optical, electronic, and thermomechanical properties monolithically in the same fiber drawn from a preform is paving the way to a new generation of multimaterial fibers endowed with unique functionalities delivered at optical fiber length scales and costs. A wide range of unique devices have been developed to date in fiber form-factor using this strategy, such as transversely emitting fiber lasers, fibers that detect light, heat, or sound impinging on their external surfaces, and fibers containing crystalline semiconductor cores. Incorporating such fibers in future fabrics will lead to textiles with sophisticated functionality. Additionally, long-standing issues in traditional applications of optical fibers have been addressed by multimaterial fibers, such as photonic bandgap guidance in hollow-core all-solid-cladding fibers and imparting mechanical robustness to soft-glass mid-infrared fibers. We review recent progress in this nascent but rapidly growing field and highlight areas where growth is anticipated. Furthermore, the insights emerging from this research are pointing to new ways that the fiber drawing process itself may be leveraged as a fabrication methodology. In particular, we describe recent efforts directed at appropriating multimaterial-fiber drawing for chemical synthesis and the fabrication of nanostructures such as nanowire arrays and structured nanoparticles.

Introduction

Optical fibers have improved the quality of life throughout the world and have fundamentally altered the human condition in both obvious and imperceptible ways. The internet, and most telecommunications, is delivered across the globe today through optical fibers.[1,2] In addition, optical fibers are used in a multitude of applications ranging from noninvasive medical surgery[3,4] to structural-integrity monitoring of bridges and oil pipelines,[5,6] and fiber lasers are finding applications in materials processing and manufacturing.[7] One of the most striking features of these advances is that optical fibers are remarkably simple devices from the perspective of materials composition. The majority of optical fibers

*raddy@creol.ucf.edu

in use today are fabricated from a single material: silica glass. While optical fibers made of other glasses or polymers have also been developed, silica glass remains the dominant material in producing optical fibers.

The mid-1990s witnessed the development of new classes of optical fibers, photonic crystal fibers (PCFs), and photonic band gap (PBG) fibers,[8] founded in new optical physics initiated with the concept of PBGs.[9] Unexpectedly, these advances were also eye-opening with regard to the perceived limitations of the structures that may be produced by the traditional process of thermal fiber drawing. In fact, the initial proposal for fabricating silica PBG fibers was dismissed as unfeasible by seasoned practitioners[10] even though no new material was combined with silica, only air holes. Nevertheless, the rapid success of PBG fibers has had unexpected consequences for the process of fiber fabrication itself. One such consequence was the introduction of the concept of "multimaterial fibers" over the past decade. This new class of fibers leverages the capabilities of traditional fiber fabrication, but aims at developing new fiber structures, functionalities, and applications that stem from altering the materials composition of the fiber. It is difficult to provide a conclusive and all-encompassing definition of this nascent concept. For the purpose of this review, we define multimaterial fibers to be *high-aspect-ratio structures that comprise multiple distinct materials, typically produced by thermal drawing from a macroscopic scaled-up model called a "preform."* Materials with different optical, electronic, thermomechanical, and acoustic properties have now been incorporated into the fiber form factor.[11] The set of fabrication approaches developed in this emerging field are introducing new functionalities that are not usually associated with optical fibers. Examples include fibers that produce an electrical signal when light is incident on the fiber external surface[12–14] or when the temperature of the ambient environment changes[15]; fibers that monitor their own performance and structural integrity[16]; flexible, lightweight fiber arrays that image the surrounding environment[14,17]; and fibers that produce or detect sound or ultrasonic signals.[18,19] Fiber drawing is therefore morphing into a fabrication route for producing electronic and optoelectronic fiber devices that may also be potentially incorporated or woven into fabrics, thereby endowing them with new and sophisticated functionalities.[11]

New ways of thinking of the fiber drawing process itself are now emerging with the advent of multimaterial fibers. Through dimensional reduction, nanostructures such as nanowires with few-nanometer diameters and unprecedented lengths may be produced.[20–23] The fiber cladding may be viewed as a crucible for chemical synthesis with the reactive agents placed in the core.[24] Multimaterial fibers are also a new playground for the controllable study of fluid dynamics in confined space and over a wide range of scales.[25] These developments have recently led to a scalable, top-down, in-fiber fabrication process capable of producing complex structured particles over an unprecedented range of diameters spanning both micro- and nanoscales.[26]

There are two aspects of fiber production that have been appropriated by the emerging field of multimaterial fibers. First, the process typically starts by preparing a macroscopic preform. As the preform diameter is on the centimeter scale, it is straightforward to create a complex transverse cross-section with controllable placement of structures incorporating multiple materials. Second, thermal fiber drawing is inherently scalable, producing kilometers of fiber with accurate control over size and axial uniformity.[27] In order for the fiber to maintain the complex transverse structure of the multimaterial preform, restrictions are placed on the allowable materials combinations compatible with this fabrication process. There are some exceptions to this overall approach. For example, multimaterial fibers may be produced starting with a single-material fiber or wire used as a scaffold for additive manufacturing, such as dip coating on the outer surface of extended fiber lengths[28] or vapor deposition inside hollow enclaves in short lengths of a preexisting fiber.[29]

While this field is still in its initial stages of development, there has been tremendous recent progress, and this review consequently aims at providing only a brief and selective overview of some of the main achievements based on our definition of multimaterial fibers provided above. The hope is that this review draws attention to this emerging field at the crossroads of optics, materials science, device physics, nanotechnology, and fluid dynamics, thereby encouraging more researchers to enter it. We first discuss in section 'Material Constraints and Fiber Drawing' some general constraints on the materials that may be codrawn in the same fiber and then describe in section 'Multimaterial Preform Fabrication' general approaches to multimaterial preform fabrication. We next describe multimaterial fibers with novel optical functionalities in section 'Photonic Multimaterial Fibers', such as transverse omnidi-

rectional emitting fiber lasers and robust composite soft-glass/polymer fibers for mid-infrared optics. In section 'Optoelectronic Fibers', we describe multimaterial fibers endowed with sophisticated electronic, optoelectronic, and even piezoelectric functionalities, in addition to recent work on producing fibers with traditional crystalline semiconductor cores. Section 'In-Fiber Synthesis' highlights novel approaches that utilize fiber drawing as a route to in-fiber chemical synthesis, while section 'In-Fiber Fluid Instabilities' discusses new insights emerging from the realization of the importance of fluid instabilities arising at the heterogeneous interfaces in a multimaterial fiber. Section 'In-Fiber Nanofabrication' reviews the use of multimaterial fibers as a route to producing nanowire arrays and structured multimaterial nanoparticles. We end the review by describing some alternative fabrication approaches (section 'Other Approaches') and future possibilities (section 'Future Prospects').

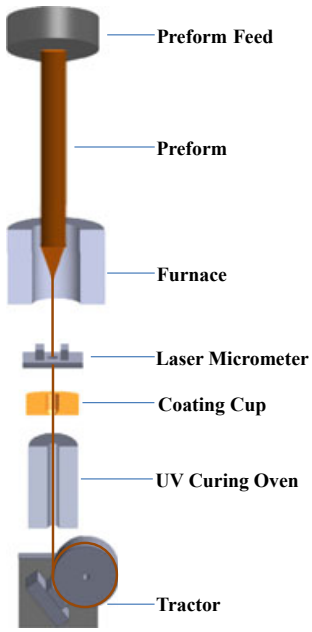

Fig. 1. Schematic of the thermal fiber drawing process in a draw tower.

Material Constraints and Fiber Drawing

Optical fibers are typically drawn thermally from a macroscopic preform in a fiber draw tower, such as that shown schematically in Fig. 1, known as the preform-to-fiber approach.[30] The preform is fed into a furnace that softens the material, after which gravity or an external force "pulls" the molten gob at the preform tip until it stretches into a thin strand whose diameter is monitored with a gauge. If necessary, polymer coatings are added to the fiber surface for mechanical protection. This relatively simple fabrication process is behind the thousands of kilometers of optical fiber used in the communications networks that span the globe today.[1,2] Alternatively, the double-crucible method[31] has been used to produce optical fibers from glass melts of the core and cladding that are pushed through a nozzle. There have been no reports to date on multimaterial fibers produced by this method.

When the preform consists of a single material, the viscosity at the drawing temperature dictates the parameters of the draw, such as the drawing speed. Multimaterial preforms, on the other hand, may contain materials that are incompatible with thermal drawing when each taken separately, such as crystalline semiconductors or metals. Using the thermal drawing process, therefore, imposes constraints on the materials combinations that are compatible with this fabrication approach. To gain insight into the feasibility of various materials combinations, we present in Fig. 2a the viscosity of silica glass, silicon, and gold as a function of temperature. These materials are chosen to represent three distinct materials classes from the electronic perspective: an amorphous insulator, a crystalline semiconductor, and a metal, respectively, in addition to their different optical and mechanical properties. The softening temperature of silica ranges from 1400 to 2350 °C, thereby offering a broad range of drawing conditions. Silicon and gold, on the other hand, are characterized by an abrupt drop in their viscosities above their melting temperature T_m, where a phase transition takes place. Nevertheless, silica may be used as a "cladding" in which a silicon or gold "core" is embedded with the preform thermally drawn above the core T_m. In this scenario, the cladding acts as a scaffold to contain and restrict the flow of the low-viscosity core material.

From this example, we may outline the general constraints on the construction of multimaterial preforms and the drawing conditions. At least one material should be amorphous, typically a glass or polymer, and resist devitrification during thermal drawing. This "backbone" material forms an outer cladding that supports the other materials during the draw and main-

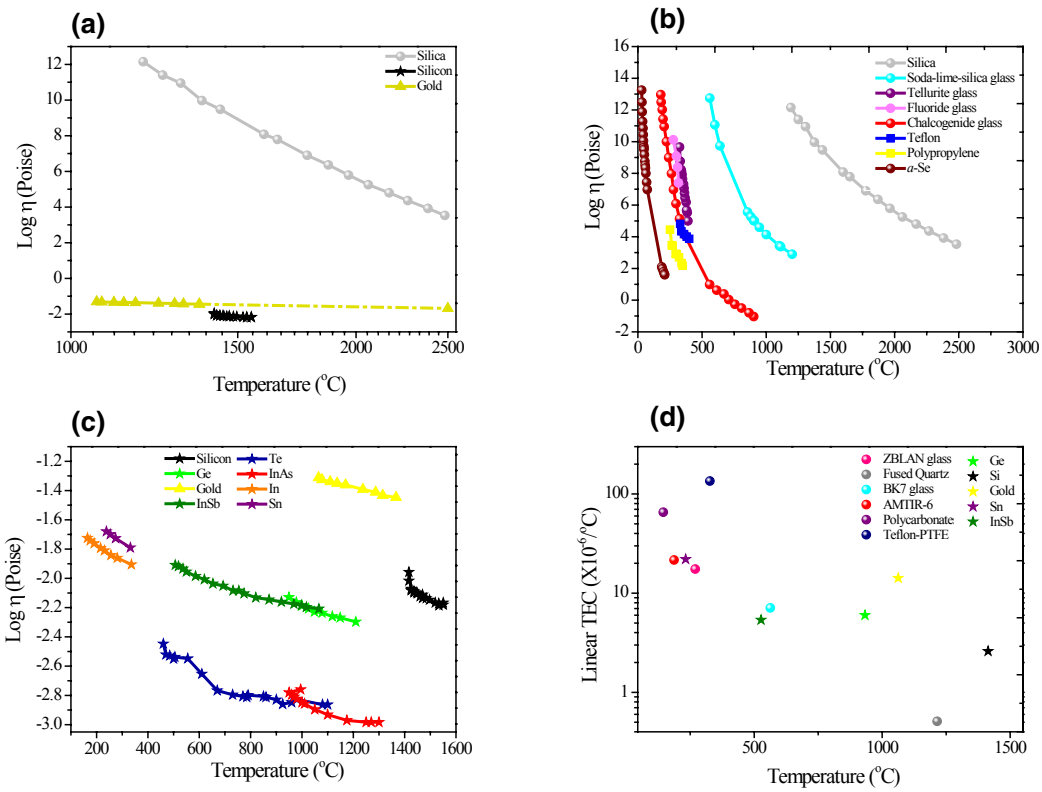

Fig. 2. Dynamic viscosity (logarithm of viscosity η in poise) of selected materials versus temperature. (a) Viscosity for silica,[32] silicon,[33] and gold.[34] The viscosity for silicon and gold are measured above their melting temperatures. (b) Same as (a), showing the viscosity for silica,[32] soda-lime-silica glass,[35] fluoride glass,[36] tellurite glass,[37] chalcogenide glass (As_2S_3),[38] Teflon® PTFE-6 polymer,[39] polypropylene (PP) polymer,[40] and amorphous selenium.[41] (c) Same as (a), showing the viscosity for silicon,[33] germanium,[42] indium antimonide,[43] tellurium,[42] indium arsenide,[42] indium,[44] tin,[44] and gold.[34] (d) Linear thermal expansion coefficient (TEC) at room temperature for selected materials plotted against the melting temperature (T_m) for metals and semiconductors (solid stars) and the glass transition temperature (T_g) for the amorphous materials (solid dots). References: Ge: T_m,[45] TEC[46]; Si: T_m,[45] TEC[47]; Gold: T_m,[48] TEC[47]; Sn: T_m,[48] TEC[49]; InSb: T_m,[50] TEC[51]; Teflon® PTFE: T_g,[52]; TEC[53]; Fused quartz: T_g,[53] TEC[54]; BK7 glass: T_g,[53] TEC[53]; AMTIR-6: T_g,[55] TEC[55]; Polycarbonates: T_g,[56] TEC[54]; ZBLAN glass: T_g,[53] TEC.[54]

tains the cross-sectional structure of the fiber. The amorphous material constituents must be chosen to have overlapping softening temperatures, while the crystalline constituents must have T_m below the drawing temperature. The drawing temperature must be lower than the boiling temperature of the core material. Additionally, care must be taken to avoid fluid instabilities that may occur when the viscosity of the materials is lowered and the transverse dimensions reduced (see section 'In-Fiber Fluid Instabilities'). The materials must also have relatively similar thermal expansion coefficients in the temperature range extending to the drawing temperature to avoid mechanical fractures resulting from thermomechanical mismatches.

In Fig. 2b we present the viscosity of a wide range of *amorphous* materials. Some glasses (such as soda-lime-silica) have a broad temperature range suitable for thermal drawing, while others (such as fluorides, chalcogenides, and tellurites) have a relatively narrower temperature window. In Fig. 2c we plot the viscosity of some typical *crystalline* materials above their T_m. Using Fig. 2b,c together, it is possible to choose potential pairs of amorphous–crystalline materials that may be combined in a preform and codrawn into a multimaterial fiber. For example, it is possible to draw Si, Ge, or gold clad with silica glass; InSb clad with soda-lime-silica glass; or Sn or Se clad with fluoride or chalcogenide glass, or even a polymer. For completeness, we identify

in Fig. 2d the glass transition temperature T_g of the amorphous materials and the melting temperature T_m of crystalline materials used in Fig. 2a–c versus the linear thermal expansion coefficient (TEC). While there are other critical aspects that must be considered in the materials selection to successfully draw a multimaterial fiber, Fig. 2 offers the basic groundwork for the potential materials pairings. Finally, we note that more than two materials chosen according to the above criteria may be incorporated in the same multimaterial fiber. This feature enables the construction of in-fiber electronic and optoelectronic devices, as described in sections 'Photonic Multimaterial Fibers' and 'Optoelectronic Fibers'.

Multimaterial Preform Fabrication

Four general classes of approaches to multimaterial preform preparation have been exploited thus far: (i) the rod-in-tube approach,[57–59] (ii) extrusion,[60–62] (iii) the stack-and-draw approach,[8,63] and (iv) thin-film-rolling technology.[11] The choice is dictated by the materials used and the transverse structure targeted.

Rod-in-Tube Approach

Figure 3a depicts the rod-in-tube approach, which relies on inserting a rod of one material into a tube of another material to form a preform with a core-cladding structure. Alternatively, a powder may be placed in the tube and the preform sealed, which enables a wide range of materials to be incorporated into the core. If T_m of the core rod/powder is lower than the drawing temperature, we designate the process molten-core-in-tube method. The recognition of the usefulness of this method for multimaterial fibers may be traced back to the pioneering work of E. Snitzer in 1989,[64]

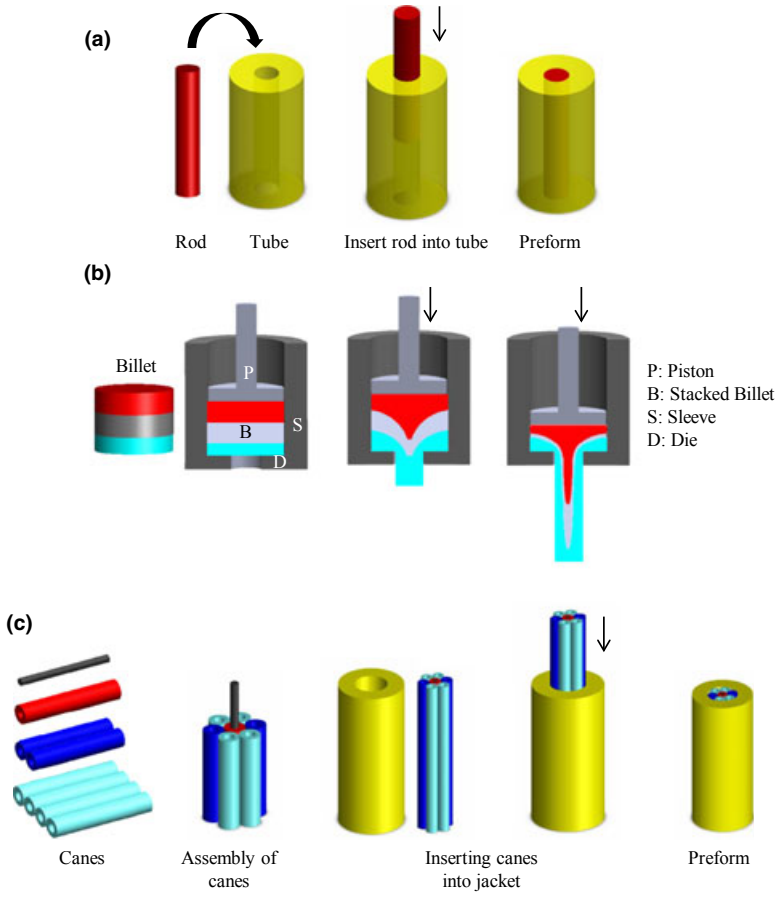

Fig. 3. General methodologies for multimaterial fiber preform fabrication. (a) Rod-in-tube, (b) extrusion, and (c) stack-and-draw methods.

where selective volatization combined with the rod-in-tube method was used to produce a silica-clad fiber containing a soft-glass core. In this work, the drawing temperature was higher than T_m of a soft-glass core, and the high vapor pressure led to the volatilization of some compounds from the core, leaving a glass core with a different residual composition.

Extrusion

Extrusion is a process used to create objects with fixed cross-sectional profile by pushing a soft material through a die under pressure. J. Bramah patented the first extrusion process for producing lead pipes in 1797,[65] and Roeder[66–68] extended this approach to soda-lime-silica, lead silicate, calcium aluminate, and boric oxide glass in the 1970s. Material in the form of a rod, typically called a *billet*, is placed inside a sleeve held in a furnace (a vertically stacked billet is shown in Fig. 3b for demonstration). The billet is heated to the softening temperature of the incorporated materials, and pressure is applied to push the material through a die that imparts shape to the extruded preform rod, which is subsequently drawn into a fiber. Using a multimaterial billet consisting, for example, of vertically stacked disks, the transverse structure of the extruded rod may be engineered.[60,62]

Stack-and-Draw Approach

The stack-and-draw approach has been used extensively in preparing the preforms drawn into microstructured fibers, PCFs, and PBG fibers.[8] The first demonstration of the stack-and-draw method to produce an optical fiber may be traced to Bell Labs in 1974,[69] at the dawn of the development of silica fibers, where a fiber containing a hanging core surrounded by air was produced. Rods, tubes, and/or plates from a single or multiple materials may be assembled into a preform (Fig. 3c) with dimensions determined by the targeted fiber structure. Multiple stack-and-draw steps may be applied recursively to reach the required dimensions and attain complex transverse structures.

Thin-Film Rolling

Polymers may be incorporated into a fiber using any of the above three approaches. A unique process to incorporate a polymer in a preform is through rolling a thin polymer film followed by thermal consolidation under vacuum above the glass transition temperature of the constituent materials until the individual films fuse. An example of this process is shown schematically in Fig. 4a, which details the fabrication approach toward making a multimaterial PBG fiber.[70–74] The thin-film-rolling technique can also be performed recursively for realizing more complex cross-sections. For example, voids may be introduced into a postconsolidated structure. These voids may be filled by conductors and

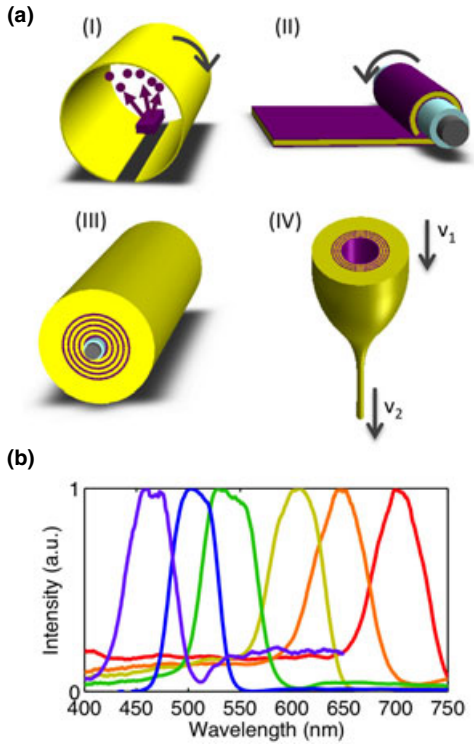

Fig. 4. PBG fiber fabrication and characterization. (a) PBG fiber fabrication flow. (I) The chalcogenide glass is thermally evaporated onto both sides of the polymer film. (II) This multilayer film is then rolled onto a teflon-lined mandrel, and additional polymer-cladding layers are rolled for mechanical support. (III) The entire structure is thermally consolidated under vacuum until the materials fuse together into one solid preform. (IV) The preform is then thermally drawn into hundreds of meters of fiber by applying uniaxial tension. The ratio of the preform down-feed speed (v_1) to fiber draw speed (v_2) dictates the final layer thicknesses. (b) Transmission band gap spectra for hollow-core PBG fibers. The fiber structure in each case is the same. The only difference is that the length of the period in the multilayer structure lining the hollow core is reduced (from right to left) resulting in the shift of the transmission PBG spectrum. Adapted from Refs. 70–74.

encapsulated in the preform by rolling additional thin films and reconsolidating. These multistep preform preparation processes form the basis for many photonic and optoelectronic multimaterial-fiber devices.[11,17,75,76]

Photonic Multimaterial Fibers

In this section, we provide an overview of multimaterial fibers used for the traditional application of light guidance axially along the fiber as well as for the novel applications for transversely active photonic fiber devices.

Multimaterial PBG Fibers

One of the first successful examples of multimaterial optical fibers was demonstrated by the MIT group led by Y. Fink. By combining two materials having a large refractive-index-contrast, PBG fibers with an all-solid cladding that guide light in a hollow core were produced, among other examples of photonic multimaterial fibers that we proceed to describe.

Hollow-core PBG fibers

A flat omnidirectional mirror, one that reflects light incident at any angle and polarization within a spectral window, can be realized using a one-dimensional (1D) periodic stack of alternating high- and low-index materials having sufficient refractive-index contrast.[77,78] This mirror can line the inner surface of a hollow-core fiber, thereby enabling axial light guidance through an air core.[79] Although premonitions of such a waveguiding mechanism have existed since the 1970s,[80] it was not until 2002 that the first multimaterial hollow-core fiber was fabricated using the standard preform-to-fiber drawing technique.[70] The challenge is twofold. First, a pair of materials must be identified that, on the one hand, have compatible thermomechanical properties, and on the other, have a high-refractive-index contrast. Second, the multilayer structure must be maintained with low-scattering interfaces down to the micro- and nanoscales for low-loss fibers to be produced. To date, several pairs of materials have been identified which yield low-loss multimaterial optical transmission fibers under appropriate fabrication conditions. A typical pair consists of a low-refractive-index polymer and a high-refractive-index chalcogenide glass, which are both amorphous and thermomechanically compatible for fiber drawing.[70–72] The fabrication process for creating hollow-core multimaterial fibers with PBGs spanning the infrared to the ultraviolet is outlined in Fig. 4a. The exquisite level of control over the layer thicknesses at the nanometer scale is demonstrated by the transmission spectra spanning the visible range (Fig. 4b) of fibers differing only in the period of the multilayer structure lining the hollow core. Such hollow-core multimaterial PBG fibers have been exploited hitherto in a variety of applications.

(1) These fibers support a multiplicity of eigenmodes.[81,82] The ability to precisely excite, propagate, and reconstruct specific modes and their superpositions [73,83,84] provides a means to sculpt and tune the vectorial field distribution along the axis of the fiber, which is important for the study of light–matter interaction over extended lengths. Moreover, as the core size decreases, the spiral nature of the multilayer structure (arising from the fabrication approach in Fig. 4a) imparts unique properties to the optical modes, resulting in asymmetric wave propagation.[85]

(2) Delivery of high-peak-power laser pulses in well-controlled spatial modes is of significant importance for many medical and industrial applications. However, the use of traditional solid-core fibers for handling high peak powers is limited owing to material absorption, which sets the damage threshold limit. Multimaterial hollow-core PBG fibers have been shown to transmit peak powers of 11.4 MW at 1.55 μm with 97% of the fiber output in the fundamental mode, a record for any fiber at this wavelength. Furthermore, PBG fibers fabricated using this approach and designed for transmitting high-power continuous-wave CO_2 laser light at 10.6 μm are routinely used as optical scalpels in minimally invasive medical procedures.[70,86]

(3) Hollow-core PBG fibers can be used for chemical vapor sensing.[74,87] For example, a chemiluminescent dye that emits light in reaction with peroxide vapor can be introduced into the fiber. In this way, the fiber provides confinement for the analyte flow and serves as an optical waveguide for transmitting the chemiluminescent signal to a remote optical detector.[74]

(4) As the transmission bandgap spectral position and linewidth depends on the core refractive index,[88,89] hollow-core PBG fibers may be used as refractive index sensors.

Radial lasing and azimuthal intensity control

The hollow core of a multimaterial PBG fiber can host a gain medium, enabling the creation of radially emitting fiber lasers that make use of the unique optical features of the PBG provided by the multimaterial Bragg structure lining the core.[76,90] This architecture is in stark contrast to all other fiber lasers, which emit light axially from their end facet. Two configurations of radially emitting fiber lasers have been explored, one incorporating an organic dye dissolved in a solid host and one in a liquid host. In both cases, the gain medium plug is introduced in the fiber core and is pumped axially as shown in Fig. 5a (left). The PBG at normal incidence to the fiber reflects the plug's fluorescence back into the core, leading to the possibility of laser action in the transverse plane. As shown in Fig. 5a (right), the radiation pattern emitted by the solid plug is anisotropic (with directionality dictated by the pump beam polarization), while the emission from the liquid is rotationally symmetric. This contrast arises from the differences in the relaxation dynamics of excited molecules in the solid and liquid phases.

The rotational symmetry and precise polarization of the radially emitting liquid laser forms the basis for a fiber device with controllable directional emission.[76] This is achieved by integrating multiple electrically controllable and individually addressable liquid-crystal-based light modulators [76] in an annular fashion around the laser cavity, as shown in Fig. 5b. These liquid-crystal-filled channels can modulate the polarized wavefront emanating from the fiber core, leading to a laser with a dynamically controlled intensity distribution spanning the full azimuthal angular range. Figure 5c depicts the laser intensity control through one of the channels as a function of the applied voltage. This new capability, implemented monolithically within a single fiber, presents opportunities ranging from flexible multidirectional displays to minimally invasive directed light delivery systems for medical applications.

External reflection fibers

Instead of lining the hollow core, the multilayer structure can also be integrated closer to the external

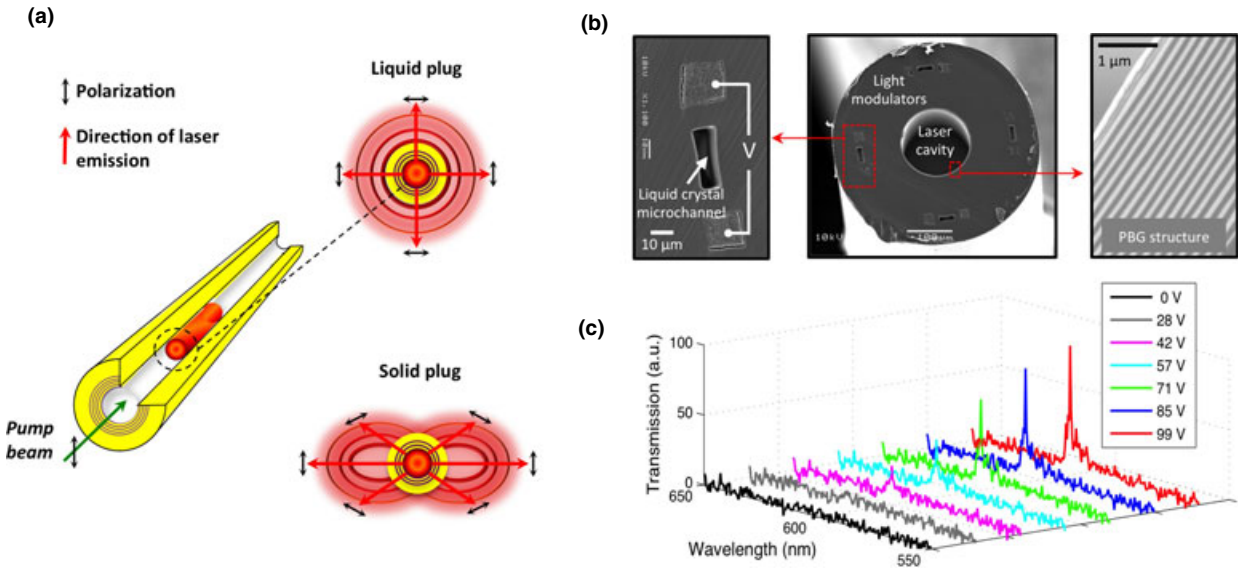

Fig. 5. Radial fiber lasers (a, left). Schematic of a radially emitting fiber laser. The red cylinder in the core corresponds to an organic-dye-doped plug, which can be a liquid or a solid. (a, right) Emission patters from the liquid plug (top) and solid plug (bottom). The red arrows denote the direction of laser emission. The direction of the lobes for the solid plug is orthogonal to the pump beam polarization. (b) Scanning electron micrograph of the hybrid fiber containing a cylindrical PBG structure encircled by four hollow channels, each flanked by a pair of conductive electrodes. (c) Laser spectra measured for light transmitted through one of the liquid-crystal-filled channels for various driving voltages. Adapted from Refs. 76, 90.

surface of the fiber, thereby creating omnidirectional externally reflective fibers.[91] While a purely periodic structure leads to photonic bandgaps which reflect light over a broad wavelength range, the intentional deviation from periodicity by introducing a defect layer facilities the existence of localized modes, which leads to narrow band transmission dips within the bandgap.[9] These narrowband cavity resonances can be tuned dynamically either by applying an axial strain to the fiber[92] or by optically modulating the defect layer via a transient photodarkening effect.[93] Incorporating such fibers into fabrics could be used for spectral-identity verification, as radiation barriers or as large-area tunable optical filters.

Multimaterial Preform Coextrusion for Robust Chalcogenide Fibers and Tapers

Combining multiple materials in a fiber may be used to improve the mechanical properties lacking in a fiber that has favorable optical properties. For example, while chalcogenide glasses have high optical nonlinearity and are transparent in the mid-infrared, the adoption of chalcogenide fibers has been limited due, in large part, to their unfavorable mechanical properties.[94] This drawback has been recently addressed through the use of one-step multimaterial coextrusion of a fiber preforms containing chalcogenide glasses and thermoplastic polymers.[62] A composite preform consisting of a chalcogenide glass core, a chalcogenide glass cladding, and a built-in polymer jacket is extruded from a vertically stacked billet into a preform that is subsequently drawn into a fiber. The polymer provides protection to the fibers during drawing and mechanical handling after drawing. Furthermore, as the chalcogenide glass and the polymer are thermally compatible, the fiber may be tapered without removing the polymer, resulting in robust, all-solid, and high-index-contrast tapers with submicrometer core diameters. These tapers have been used to produce octave-spanning infrared supercontinuum spectra using picosecond pulses at 1.55 μm.[95]

A cross-section of such a fiber, which is drawn from the preform extruded from the billet in Fig. 6a, is shown in Fig. 6b.[62] The fiber outer diameter is 1 mm, and the chalcogenide glass represents <1% of the fiber volume (Fig. 6c). Figure 6d demonstrates the robustness of such fibers. Additionally, the large index contrast between core and cladding allows for the strong confinement of the optical radiation in the core, preventing it from reaching the polymer cladding and also enhancing nonlinearities.[95] This unique fabrication procedure thus enables substantial flexibility in designing chalcogenide glass fibers while imbuing the fibers with excellent mechanical properties not available in all-glass fibers produced using standard approaches.

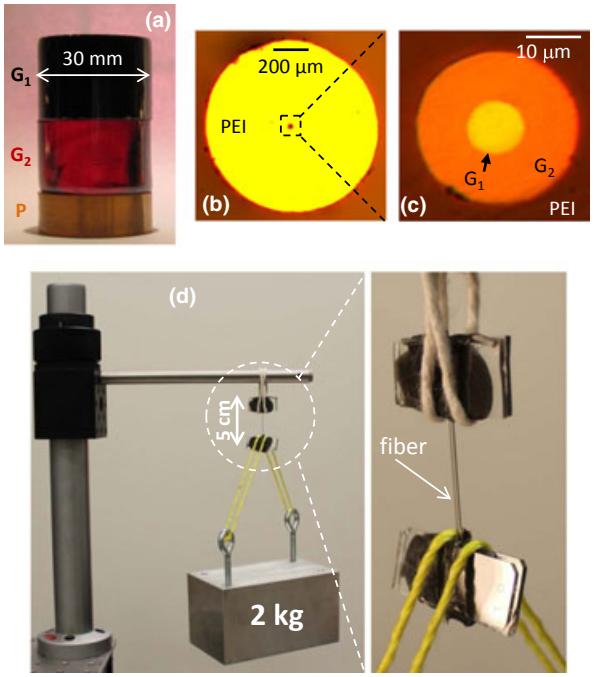

Fig. 6. Robust mid-infrared fibers. (a) Vertically stacked billet to produce a preform. (b) Transmission optical micrograph of the fiber cross-section, and (c) reflection micrograph of the core. P: polyetherimide (PEI) polymer; G_1: As_2Se_3; G_2: As_2S_3. (d) A 2-kg weight hanging from a 5-cm-long fiber demonstrating the mechanical strength of the multimaterial fiber. The inset shows the hanging mechanism.[62]

Other Examples of Multimaterial Optical Fibers

The idea of combining glasses with polymers in an optical fiber has been investigated since the 1980s[96–99] to appropriate the favorable mechanical properties of polymers to compensate for the less-favorable mechanical properties of fluoride and chalcogenide glasses. Thermal codrawing of these glasses with polymer jacket, such as Teflon, greatly improves the mechanical properties of the fiber. In 1981, S. Shibata and T. Manabe reported the fabrication of fluoride-glass-core polymer-cladding fibers[99] from a rod-in-tube preform.

In 1984, *NTT* scientists[98] reported similar research using a chalcogenide glass. Infrared fiber bundles were fabricated using the stack-and-draw approach by *Horiba Ltd*[100,101] in the 2- to 6-μm spectral window, see also Refs. 102,103. The Naval Research Laboratory (NRL)[104] also developed glass/polymer multimaterial-fiber fabrication technology using the rod-in-tube method in the 1990s.

The ability to combine different optical glasses in a fiber and exploiting the contrast in their optical properties can be beneficial in dispersion control and engineering the fiber optical nonlinearities. A fiber consisting of a chalcogenide glass core in a tellurite glass cladding (produced by the stack-and-draw method)[63,105,106] was shown to have flattened chromatic dispersion and a zero-dispersion wavelength shifted to the near infrared, enabling supercontinuum generation covering 800–2400 nm. Additionally, all-solid PBG-guiding PCFs consisting of a hexagonal lattice of high-index soft-glass strands embedded in a low-index soft glass[107] (produced by the stack-and-draw method) have been investigated. In practice, this approach is limited by the availability of pairs of glasses with overlapping softening temperatures and thermal expansion coefficient. More research is needed to fully exploit the opportunities enabled by these multimaterial optical fiber structures.

Optoelectronic Fibers

Metal-Insulator-Semiconductor Fibers

The creation of electronic and optoelectronic devices requires the assembly of metals (M), insulators (I), and semiconductors (S), in prescribed geometries with low-scattering interfaces and nanoscale feature sizes. While traditional wafer-based approaches have been applied to this problem, they are limited to primarily rigid and low-aspect ratios structures. However, if all the constituent device components could be integrated into a fiber, the complex functionality associated with modern chip-based devices could extend into flexible and weavable/wearable fabrics.

Several M-I-S fiber structures have been created thus far. Figure 7a depicts an M-I-S preform being elongated into a fiber, and a corresponding scanning electron microscope (SEM) images of the cross-section is shown in Fig. 7b.[12] This fiber produces an electrical signal proportional to the optical power incident on its external surface when the electrodes are connected at the fiber periphery to an electrical circuit. Two advantages are gained by reducing the bulk semiconductor cylinder to a thin-film structure such as shown in Fig. 7c.[13] First, the dark current, which sets the noise level for optoelectronic applications, is reduced by more than an order of magnitude. Second, the creation of thin-film structures enables higher device-density per fiber (Fig. 7d) as well as more elaborate geometries (Fig. 7e).[17] All of these structures are axially symmetric, with the electrodes forming intimate contacts with the semiconducting chalcogenide glass layers along the entire fiber length. Postdraw the electrodes can be contacted through the fiber cladding or by wire bonding to the end fiber facet and connected to an external driving circuit.

Both the composition of the semiconducting chalcogenide glass and the geometry of other structural elements comprising the preform can be tuned to target particular applications.

(1) Using a photoconductive glass, photodetecting fibers are created with the ability of detecting illumination along their entire length,[12,13,17,108] which has applications spanning chemical vapor sensing[109] to lensless imaging.[14,17] Each pair of adjacent electrodes can act as an independent photodetector, thereby imparting increasing functionality. For example, a semiconductor ring structure (Fig. 7c) can be used to determine the angle of incidence of an incoming beam in the plane perpendicular to the fiber axis. Moreover, the semiconductor's wavelength-dependent absorbance may be leveraged using a duel ring structure (Fig. 7d) to reconstruct the wavelength of an incident beam by measuring the ratio of photocurrents in the inner and outer rings.
(2) Photoconductive glasses typically respond over a broad wavelength range. To impart spectral selection to a photosensitive fiber, a multilayer reflector containing a defect cavity can be combined with a photodetecting structure.[12] The thickness of the defect cavity determines the narrow band transmission window within the PBG, allowing the engineering of spectroscopic photosensitive fibers tuned to respond at specific wavelengths.
(3) A heat-sensitive semiconductor with a temperature-dependent conductivity can be drawn into a fiber with the identical geometry as shown in

Fig. 7b, but with the ability to detect changes in temperature along its entire length.[15] Integrated into fabrics, such fibers can be used for temperature sensing over large areas. Moreover, a thin-film ring of the same semiconductor can be integrated into a PBG transmission fiber to predict the onset of fiber failure.[16]

(4) The electronic properties of the semiconductor can also be significantly altered postdraw by crystallization. This method has been used for realizing in-fiber field-effect transistors[110] and rewritable memory devices reminiscent of the ovonic switch.[111]

Meters of fiber result from a single draw (Fig. 7f), thus facilitating the construction of large-area assemblies and fabrics with optoelectronic, thermal, and acoustic functionalities. For example, two grids of photodetecting fibers cascaded one after another (Fig. 7g) can reconstruct the direction of an optical beam and be used for lensless imaging. Moreover, the wavelength-reconstruction property of dual-ring fiber structures (Fig. 7d) enables a single fiber grid to perform lensless imaging,[17] thus opening the possibility for fabrics that can see.

One path for introducing rapid modulation into the optical properties of a fiber is through the piezoelectric effect. This can be achieved by drawing a copolymer, P(VDF-TrFE), that has a stable beta-phase at room temperature, and therefore will directly crystallize from the melt into the piezoelectric phase. Two fiber geometries have been investigated as shown in Fig. 8a, b, and measurements confirm that the fibers can both emit and detect acoustic radiation over a broad acoustic frequency range spanning the kHz to MHz.[18] The cross-sectional fiber geometry dictates the acoustic radiation emission pattern, as shown in Fig. 8c. Arrays of piezoelectric fibers can be constructed leading to sophisticated functionalities such as coherent acoustic wave interference and beam steering,[19] and large-area acoustic fiber webs, such as that depicted in Fig. 8d, pave the way toward novel applications ranging from large-area pressure wave monitoring to communications.

Crystalline-Semiconductor-Core Fibers

With the success in endowing fibers with electronic and optoelectronic functionalities through the use of

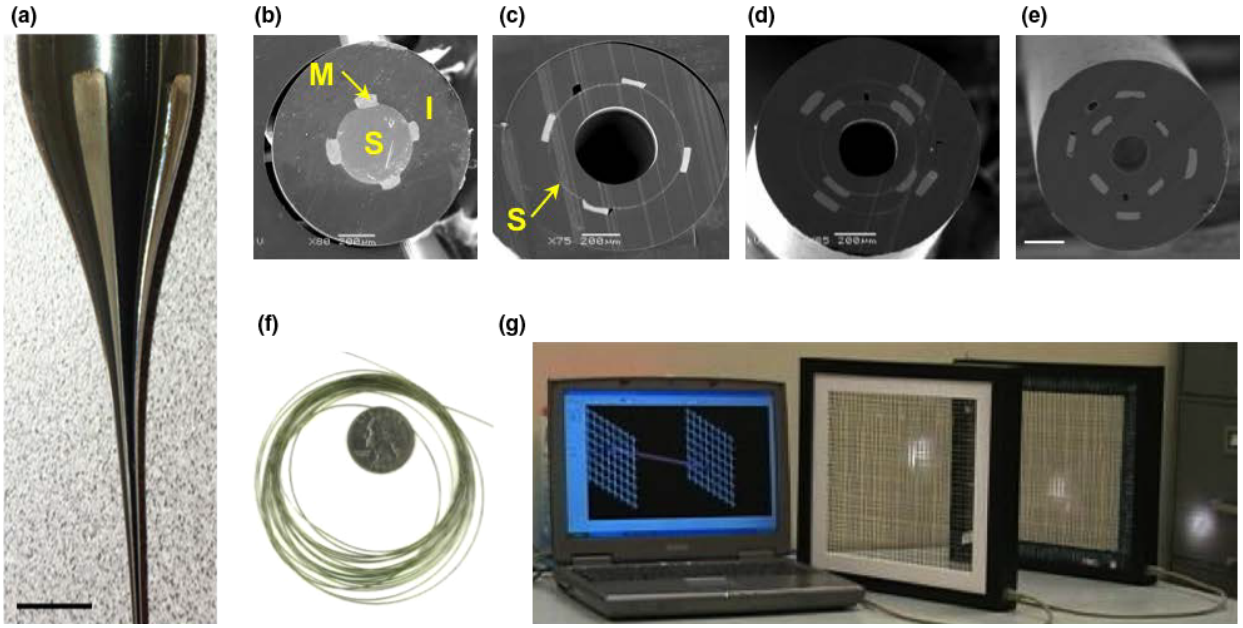

Fig. 7. Metal (M)–insulator (I)–semiconductor (S) Fibers (a) Picture of an M-I-S preform scaling down into a fiber. (scale bar is 1 cm). (b–e) SEM micrographs of various M-I-S fiber architectures. (Scale bar from left to right: 200, 200, 200, 100 μm). (f) Several meters of coiled fiber. (g) Two fiber grids made of photoconductive fibers are connected to the computer. A flash light beam passes through both grids, and the directionality of the beam is reconstructed as seen on the computer monitor. Adapted from Refs. 11–17.

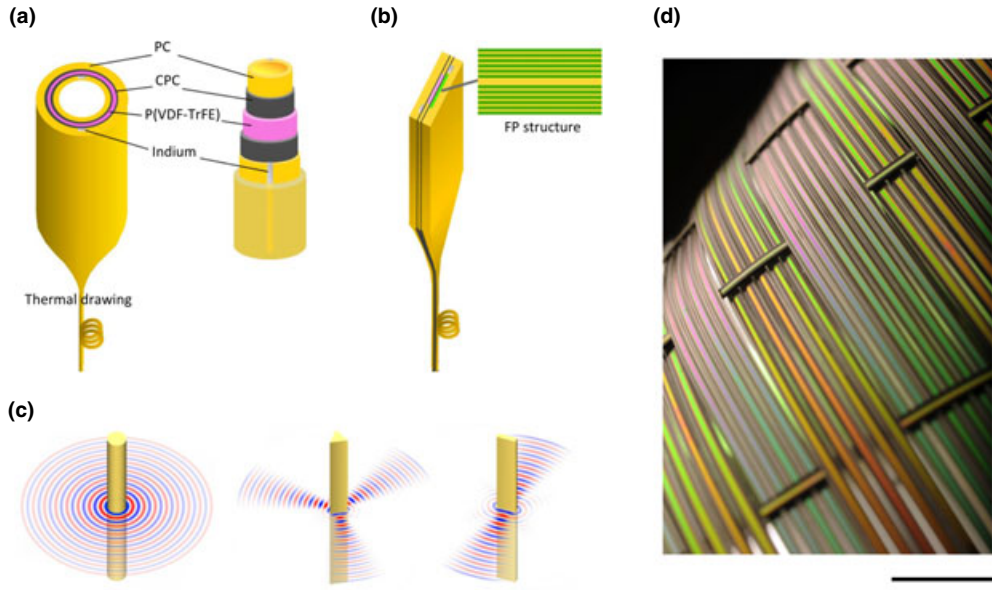

Fig. 8. Piezoelectric fibers. (a) Schematic showing the assembly of a cylindrical piezoelectric preform. (b) Schematic of a rectangular piezoelectric preform with an integrated Fabry–Perot (FP) cavity structure. Both structures have been successfully fabricated and function as acoustic sensors and actuators. (c) Near-field pressure patterns of the acoustic emission at 1.3 MHz from a circular fiber, a triangular fiber and a rectangular fiber with cross-sectional dimensions of about 2 mm. (d) Two-dimensional device fabric constructed by knitting the piezoelectric/FP fibers as threads. The colors in the fabric are because of reflections from the FP optical structure embedded in the fibers (scale bar is 1 cm).[18]

amorphous semiconducting glasses, it is natural to ask whether such fabrication strategies may be extended to traditional semiconductors, such as silicon and germanium, that are the mainstay of the electronics industry. Silicon (Si) and germanium (Ge) are also attractive for their optical properties: They are transparent in the mid-infrared, have high optical damage threshold,[112,113] and are also highly nonlinear.[114,115] For example, the Raman gain coefficient in Si is ~10^4 times greater than that of silica. Furthermore, the high thermal conductivity of Si and Ge offers opportunities in better removal of dissipated heat. The extension from planar substrates to optical fibers[29,57] is therefore a significant complement to the emerging field of silicon photonics.[116–119]

There has been significant recent progress in developing fibers containing traditional crystalline semiconductors. The first thermally drawn Si-core optical fiber was demonstrated by J. Ballato's group in 2008[57] (Fig. 9a) using the molten-rod-in-tube method. As T_m of Si (~ 1416 °C) overlaps with the softening temperature of silica (Fig. 2a), such a materials combination in a multimaterial fiber is feasible from a thermal compatibility standpoint. A Si rod (3 mm diameter, 40 mm length) is inserted into a thick-walled silica tube. The assembled preform is drawn into tens of meters of fiber with core diameters cladding. This approach has been extended to several other semiconductors such as Ge[120,121] and InSb,[122] among others. Figure 9b is a scanning electron micrograph of a Ge-core optical fiber.[120] Attempts at producing crystalline fiber cores from more crystallographically complex systems, such as erbium-doped yttrium aluminum garnet (YAG), have not yet been demonstrated conclusively.[123]

Although this fiber is extremely simple from an elemental-analysis perspective (Si and O are the only two elements involved), this glass/crystalline-semiconductor materials system has nevertheless proven very fruitful in fundamental studies of diffusion and crystallization in confined volumes. Extensive work by J. Ballato's group, using X-ray diffraction, Raman spectroscopy, and spatially resolved crystallographic orientation studies,[121,124] have elucidated the polycrystalline domain structure of the core along the fiber. Several approaches have been exploited to increase the axial length of the single-crystal domains, including

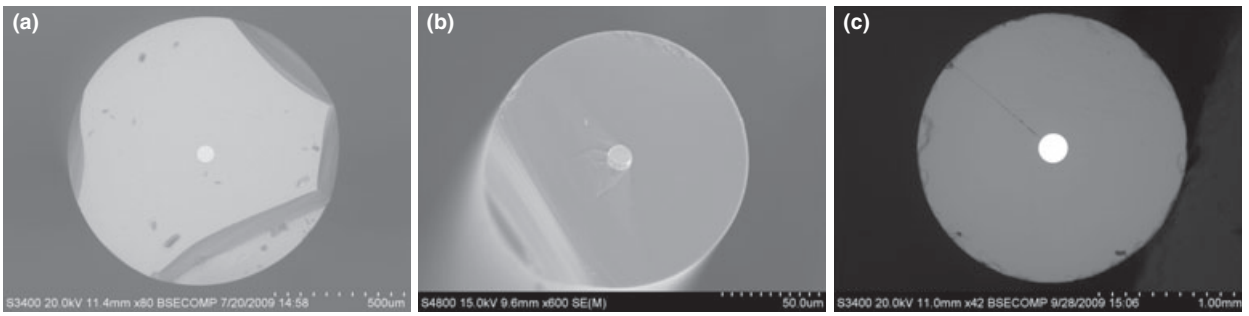

Fig. 9. Crystalline semiconductor core fibers. (a) Scanning electron microscope (SEM) micrograph of the core region of the silicon core, silica-clad optical fiber in Ref. 57. (b) SEM micrograph of a crystalline Ge core optical fiber from Ref. 120. (c) SEM micrograph of a crystalline InSb core fiber (courtesy of Prof. J. Ballato).

fiber-annealing by rapid photothermal processing (RPP) and controlling the core geometry,[125] which have led to larger single-crystal domains. It is expected that such approaches will yield fibers with improved structural, electrical, optical, and mechanical properties.

Another research effort to produce Si-core fibers using the powder-in-tube method is reported in Ref. 58. Silicon powder is packed into a silica tube which is then evacuated to limit the oxidation of Si. Outer diameters in the range of several hundred microns and core diameters in the range of tens of microns of n-type Si optical fibers have been demonstrated by this method.[58] High optical losses have been observed, which are attributed to irregularities along the fiber, such as thermal-expansion-induced microcracks at the core/cladding boundary and the polycrystallinity of the Si core.

This area of research is expected to blossom in the next few years with more research groups entering this field. While the focus to date has been on the materials science aspect of this class of multimaterial fibers, it is anticipated that the maturation of this field will lead to the development of fibers endowed with electronic and optoelectronic functionalities having potential applications in functional clothing and solar energy harvesting.

In-Fiber Synthesis

The high temperatures associated with thermal fiber drawing and the potential of using core and cladding materials with very different chemical reactivity suggests the possibility of exploiting fiber drawing in chemical synthesis. In this context, the preform cladding is viewed as a crucible in which a chemical synthesis process is confined. During fiber drawing, physical changes first take place, such as a reduction in the core and cladding viscosity, and potentially melting or volatization of the core. In the in-fiber synthesis approach, these *physical* changes are then followed by *chemical* changes where new compounds are produced in the core, either by reactions between preexisting core compounds or through diffusion of elements or compounds from the cladding into the core. This is an example of a re-imagining of the fiber drawing process itself, where the elongation at high temperature of multimaterial fibers is used to achieve a new goal: controlled chemical reactions along an extended length in confined space.

The multimaterial in-fiber synthesis concept may be traced to work by E. Snitzer and R. Tumminelli in 1989[64] described in section 'Multimaterial Preform Fabrication'. The drawing temperature of the fiber was higher than that of the core soft-glass T_m, and its higher vapor pressure in the liquid phase led to the volatization of some compounds in the hot neck-down region resulting in a different residual core composition. This pioneering work can also be viewed as the first instance of drawing two families of materials having incompatible thermal properties.

More recently, low-temperature materials ($Se_{97}S_3$ and $Sn_{85}Zn_{15}$) were codrawn and a ZnSe compound was produced in the drawn fiber.[24] A surprising feature is that the produced compound (ZnSe here) has a much higher melting temperature than that of the drawing process. Ballato *et al.*[126] used as-purchased crystalline Bi_2O_3-rich (Bi_2O_3 + GeO_2) and $Bi_{12}GeO_{20}$ powders (core) placed in borosilicate glass tube

(cladding) to produce fibers where an *in situ* reactive chemical synthesis takes place during the drawing process in both amorphous and crystalline cores. This processing route can be used potentially for core materials that are difficult to fabricate or machine into a rod using conventional methods. Furthermore, in an attempt to reduce the diffusion of oxygen from the silica cladding to the Si core, silicon carbide (SiC) was introduced into the core to provide an *in situ* reactive oxygen getter during the drawing process[127] through the reactive-molten-core method.

In-Fiber Fluid Instabilities

During thermal drawing, the viscosity of the drawn materials is reduced. A multimaterial fiber preform is thus a complex fluid dynamical system. In the neck-down region where the diameter of the large preform is reduced to that of the drawn fiber, the constricted flow of the materials may be compared to the flow of a jet out of a nozzle. The controllable reduction in feature sizes within a multimaterial fiber therefore potentially allows fluid instabilities to develop at the heterogeneous interfaces. Although such phenomena are universal and ubiquitous, they lay dormant during the development of traditional silica fibers for several reasons. First, as the core and cladding are very similar materials (usually the same glass with different dopants), there is very little surface energy at the interface. Second, the high viscosity of silica glass helps arrest the development of fluid instabilities. Third, the high drawing speed results in a small dwelling time in the low-viscosity state, which is typically much shorter than instability growth times. Finally, the core diameter is relatively large (hence the curvature is small), which reduces surface energy. Nevertheless, some applications that demand extremely high axial uniformity, such as phase-matching for four-wave mixing across a wide bandwidth, are limited by the nanoscale fluctuations along the fiber.[128] In PBG fibers, it has been realized that capillary waves frozen at the free silica/air interfaces cause optical scattering that increases optical transmission losses.[129] In multimaterial fibers, it is expected that such instabilities will be even more significant as high surface energy may exist at the heterogeneous interfaces and the nanoscale features result in high surface curvature that increases the surface energy. We review here two such instabilities that have been studied recently in multimaterial fibers.

Fluid Instabilities in a Thin Film Embedded in a Multimaterial Fiber

The wavelength of light confined in a hollow fiber core lined with a 1D cylindrical multimaterial periodic structure is determined by the refractive indices and the length of the period.[78] Guiding visible or UV light therefore necessitates reducing the thicknesses of the layers to a few tens of nanometers. An obvious question is the following: What is the thinnest such layer that may be produced stably via thermal drawing from a multimaterial preform? This question was investigated in Ref. 20 by drawing amorphous As_2Se_3 and Se thin films of various thicknesses embedded in polyethersulfone (PES) and polysulfone (PSU) polymer claddings, respectively. It was observed that the initially intact cylindrical thin-film breaks up along the azimuthal direction into an array of wires that are axially continuous. The film thickness at which this breakup process occurs, which consequently determines the diameter of the resulting wires, depends on the materials combination. For As_2Se_3/PES, this breakup occurred below 10-nm film thickness; while for Se/PSU it occurred at 100 nm. The fluid dynamical origin of this striking phenomenon has been investigated from a theoretical standpoint,[130] but firm conclusions have not yet been reached.

Fluid Instabilities in a Cylindrical Core Embedded in a Multimaterial Fiber

A second fluid instability occurring along the *axis* of a multimaterial fiber has recently been reported (Fig. 10).[25] In this case, a drawn multimaterial fiber consisting of a cylindrical core embedded in a cladding (Fig. 10a–c) is thermally treated. It was observed that heating the fiber for a sufficient period of time results in the initially intact core breaking up into a necklace of uniformly sized spheres along the fiber axis. This is a manifestation of the classical Plateau–Rayleigh capillary instability (PRI), the general tendency of fluid threads to break up into spherical droplets. As temperature increases, the viscosity of the fiber materials drops and surface tension at the heterogeneous interfaces dominates. Thermodynamically driven fluctuations arise at the interfaces, and certain fluctuation wavelengths, determined by the relative viscosity of the two materials and their surface energy, grow without bound. These wavelengths are observed as a sinusoidal modulation

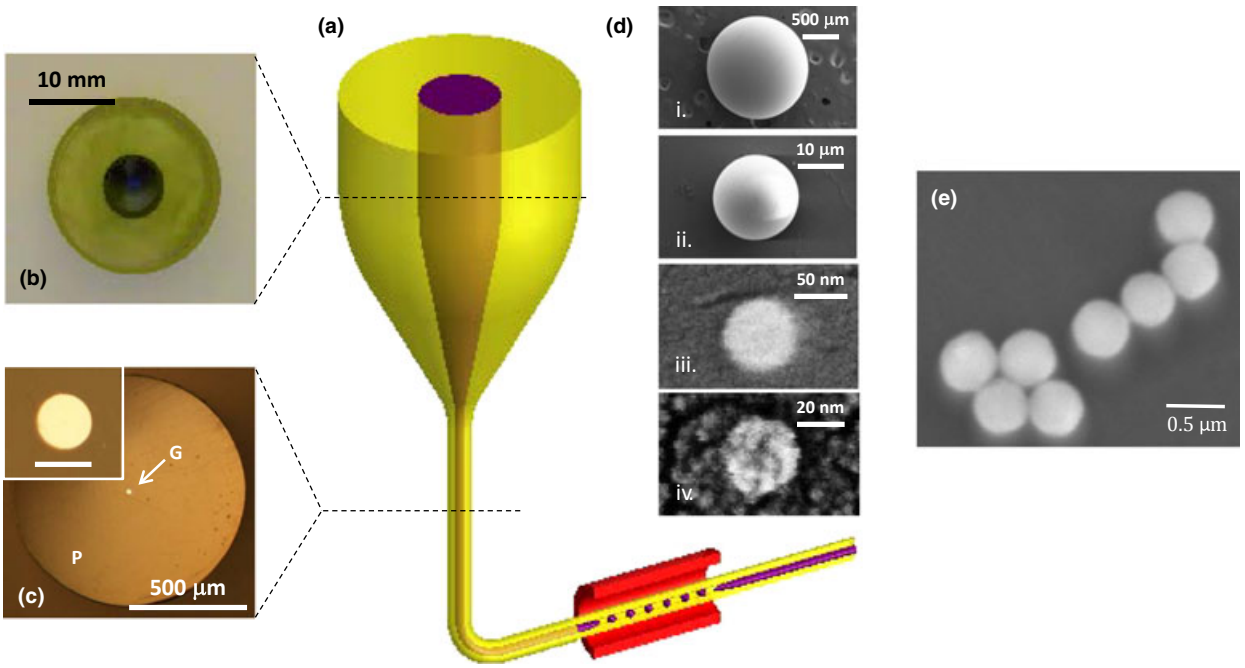

Fig. 10. Fluid capillary instabilities in multimaterial fibers as a route to size-tunable particle fabrication. (a) A macroscopic preform is thermally drawn into a fiber. Subsequent thermal processing of the fiber induces the PRI, which results in the breakup of the intact core into spherical droplets that are frozen in situ upon cooling. (b) Photograph of a preform cross-section. The core is the amorphous semiconducting chalcogenide glass As_2Se_3, and the cladding is the thermoplastic polymer PES. (c) Reflection optical micrograph of a fiber cross-section with 20-μm-diameter core; inset shows the core (scale bar, 20 μm). The fiber consists of an As_2Se_3 glass core G, encased in a PES polymer cladding P. (d) SEM images of particles with diameters: i. 1.4 mm, ii. 18 μm, iii. 62 nm, and iv. 20 nm. Adapted from Ref. 26. (e) SEM images of Si spheres created by inducing a fluidic instability in Si-core/silica-clad fibers.[133]

that develops at the core/cladding interface. The modulation depth at this instability wavelength increases until the cylindrical intact core breaks up into an array of spherical droplets. Using the classical Tomotika model[131] of the PRI, excellent agreement has been found between measurements and calculations.[25,26]

From the above we see that multimaterial fibers may be used to explore fluid dynamical problems at a wide range of length scales, and in ranges of parameters and classes of materials inaccessible to traditional micro- and nanofluidic approaches. We anticipate that this line of research will witness considerable growth in the next few years.[26]

In-Fiber Nanofabrication

The ability to reduce the transverse dimensions of complex features and structures from a multimaterial preform to a fiber suggests fiber drawing as a route to nanofabrication. A multitude of potential structures may be produced in this fashion, and we will describe two here to give a flavor of this research direction.

Nanowires from a variety of materials have been produced using the fiber drawing process at length scales inaccessible to traditional vapor–liquid–solid processes typically used in producing nanowires. Recent work has demonstrated that amorphous and postdrawing-crystallized nanowires may be produced down to a few-nm diameter. Nanowires of amorphous Se and As_2Se_3 were produced starting from a thin film[20] (see section 'In-Fiber Fluid Instabilities'). In Ref. 23 single-material and core-shell nanowires were produced, and color-control was demonstrated using a two-component nanowire in Ref. 132. The limit of this process was investigated,[23] and thermal drawing of amorphous As_2Se_3 nanowires with sub-5-nm diameters has been demonstrated. The stack-and-draw process allows for

large, well-ordered, macroscopic arrays of nanowires to be readily assembled in a fiber that may be handled manually.

As we saw in the previous section, capillary instabilities (such as the PRI) may be controllably excited in multimaterial fibers via thermal treatment. While such fluid instabilities may be viewed as an obstacle to size reduction, they may also be viewed both as an opportunity to study fluid dynamics in new geometries and also as a fabrication methodology to produce micro- and nanostructures, such as spherical structured nanoparticles. There is a wide range of applications of micro- and nanoparticles, ranging from drug delivery to cosmetics that require efficient scalable pathways for producing particles over a wide range of sizes, from a variety of materials, and in a multitude of different structures. It has been recently demonstrated that an in-fiber PRI, coupled with the inherent scalability of fiber production, enables the fabrication of uniformly sized, structured spherical particles spanning an exceptionally wide range of sizes: from 2 mm down to 20 nm (Fig. 10d).[26] The particles resulting from the PRI initiated by thermal treatment of the fiber are frozen *in situ* upon cooling the fiber, after which the particles are released when needed (see Fig. 10d). By judiciously designing the preform, the fabrication of composite, structured, spherical particles, such as core–shell particles, bicompartmentalized "Janus" particles, and multisectioned "beach ball" particles were produced. Moreover, the process is made scalable by producing fibers with a high density of cores, which allows for an unprecedented level of parallelization.[26] Research efforts are also underway for inducing capillary breakup of Si cores in silica-clad fibers into periodic arrays of nanoscale Si spheres, which may be released from the cladding (see Fig. 10e).[133]

Other Approaches

We have described in the previous sections various multimaterial fibers that have been produced using the general methodology of preform-to-fiber fabrication. There are some interesting exceptions that we present briefly in this section. The first is an approach developed by Konarka, Inc., which starts from a long steel wire that is used in successive steps of dip-coating in organic solutions.[28] The result is a fiber with a multilayer coating along its whole length, forming an organic photovoltaic cell with ~3% efficiency. The second approach uses a silica fiber with hollow enclaves (either a hollow-core fiber or a PCF) as a scaffold for vapor deposition of traditional crystalline semiconductors, a process typically called high-pressure microfluidic chemical deposition (HPMCD)[29] that extends the materials that may be incorporated into the fiber to single-crystal semiconductors[134] and polycrystalline elemental or compound semiconductors.[122,135] High-pressure flow (2–1000 MPa) is used in silica microstructured optical fibers (MOFs) to overcome mass-transport constraints, resulting in uniform, dense, and conformal annular deposition onto hollow pore walls with uniformity on the order of 0.1 nm. Such an approach thus combines two well-developed fabrication methodologies, chemical vapor deposition (CVD),[136] and silica fiber drawing. The basic idea is shown in Fig. 11a, which involves heating small quantities of a high-pressure precursor within the interior of a MOF that decomposes upon heating to deposit on the walls in an amorphous state to ensure that it bonds smoothly, followed by annealing for crystallization. Figure 11b is an example of deposited doped semiconductor layers and metals.[137] As the annular deposited film grows thicker, the central holes from which depositions occurs becomes smaller until it is completely plugged and flow is extinguished. The empty pores in the MOFs are thus treated as micro- or nanoscale reaction chambers. A fiber-based device fabricated using this approach enabled all-optical modula-

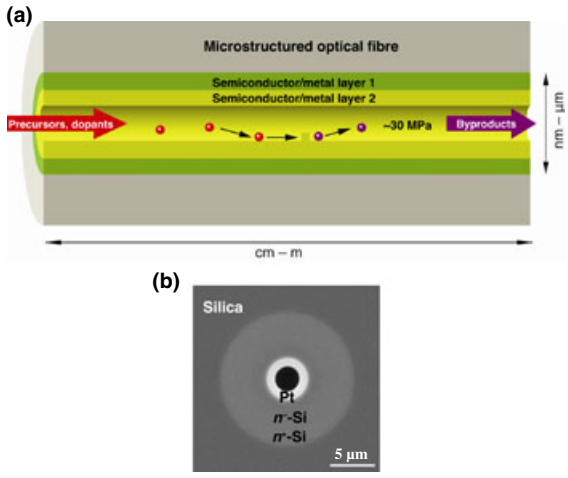

Fig. 11. Integration of semiconductor junctions in MOFs. (a) Illustration of HPCVD in a MOF pore. (b) A Pt/n^--Si Schottky junction formed by sequential deposition of phosphorous doped n^+-Si, n^--Si and platinum layers.[137]

tion of 1.55-μm guided light via free-carrier absorption mediated by a 532-nm pump pulse.[138] Other examples include producing a ZnSe-core fiber,[135] in-fiber Si and Ge wires and tubes used as field effect transistors,[139] and in-fiber crystalline Si p–n homojunctions and Pt/n-type Si heterojunctions.[137] The HPCVD technique can accommodate different capillary core dimensions and may also be used to fill a large number of micro- and nanoscale pores in MOFs. The main drawback of this technology is the limited lengths of fiber devices produced compared to those resulting from fiber drawing.

Future Prospects

We hope to have presented an overview of the wide range of exciting ideas currently investigated in the nascent field of multimaterial fibers. The field has grown dramatically over the past decade, and it is impossible to cover all the ideas being explored in this brief review. One such omission is recent work on producing multimaterial-fiber metamaterials.[140–144] Metamaterials are synthetic photonic structures that enable exotic optical phenomena such as cloaking.[145] By drawing arrays of metallic structures in a polymer fiber, it has been possible to demonstrate control over the electrical and magnetic resonances experienced by THz radiation transmitted through the transverse fiber cross-sections. Extending this approach to optical wavelengths will require further reduction of the feature sizes in the multimaterial fibers while avoiding in-fiber fluid instabilities (section 'In-Fiber Fluid Instabilities'). Other examples include the use of gold in silica fibers for plasmonic studies and the use of soft glasses inside silica fibers for mid-infrared nonlinear applications[146–153] and sapphire-derived all-glass optical fibers with engineered Brillouin scattering properties suitable for sensors and high-energy fiber laser applications.[154]

Further research is needed to increase the density of optical, electronic and optoelectronic devices incorporated in a multimaterial fiber. Producing fibers endowed with such functionalities in a form that may be directly woven into fabrics would be a milestone for this field, leading to a marriage of optics, electronics, and textiles. Using in-fiber capillary instabilities to produce three-dimensional macroscopic synthetic photonic structures with nanoscale control over the material distribution will enable unprecedented control over the behavior of light and sound. No doubt, further surprises lie ahead. It is safe to say that the progress in multimaterial fibers reviewed here is pointing to a renaissance in fiber fabrication that promises to continue for a long time to come.

Acknowledgments

The authors would like to acknowledge Yoel Fink and John D. Joannopoulos for their encouragement, support, and vision. We thank John Ballato, Siddharth Ramachandran, Steven G. Johnson, Daosheng S. Deng, and Guifang Li for useful and illuminating discussions. We also thank Yan Zhang, Yifan Liu, Tiansi Wang, Fang Chen, Cen Xia, and Zhiyong Yang for their assistance in preparing this review. This work was supported by the U.S. National Science Foundation under award number ECCS-1002295, the NSF Materials Research Science and Engineering Program under award number DMR-0819762, and in part by the U.S. Air Force Office of Scientific Research (AFOSR) under contract FA-9550-12-1-0148.

References

1. G. P. Agrawal, *Fiber-Optic Communication Systems*, 4th Edition, John Wiley & Sons, Inc., Hoboken, NJ, 2010.
2. R. Ramaswami, K. N. Sivarajan, and G. H. Sasaki, *Optical Networks: A Practical Perspective*, 3rd Edition, Morgan Kaufmann Publishers Inc., San Francisco, CA, 2009.
3. J. I. Peterson and G. G. Vurek, "Fiber-optic Sensors for Biomedical Applications," *Science*, 224 123–127 (1984).
4. A. G. Mignani and F. Baldini, "Biomedical Sensors Using Optical Fibres," *Rep. Prog. Phys.*, 59 1–28 (1996).
5. Z. Zhou, J. He, M. Huang, J. He, and G. Chen, "Casing Pipe Damage Detection with Optical Fiber Sensors: A Case Study in Oil Well Constructions," *Adv. Civil Eng.*, Article ID 638967, 9 pages, 2010.
6. N. Mohamed, I. Jawhar, J. Al-Jaroodi, and L. Zhang, "Sensor Network Architectures for Monitoring Underwater Pipelines," *Sensors*, 11 [11] 10738–10764 (2011).
7. T. Webber, "Advances in Fiber Lasers for the Materials Processing Market," Quantum Electronics and Laser Science Conference (QELS) on Advances in High-Power Lasers and their Applications III: Processing (JTh4I), San Jose, CA, May 6, (2012).
8. P. Russell, "Photonic Crystal Fibers," *Science*, 299 358–362 (2003).
9. J. D. Joannopoulos, S. G. Johnson, J. N. Winn, and R. D. Meade, *Photonic Crystals. Molding the Flow of Light*, 2nd edition, Princeton University Press, Princeton, NJ, 2008.
10. P. Russell, "Photonic Crystal Fibers: A Historical Account," *IEEE LEOS Newsletter*, 21 [5] 11–15 (2007).
11. A. F. Abouraddy *et al.*, "Towards Multimaterial Multifunctional Fibres that See, Hear, Sense and Communicate," *Nat. Mater.*, 6 336–347 (2007).
12. M. Bayindir, F. Sorin, S. Hart, O. Shapira, J. D. Joannopoulos, and Y. Fink, "Metal-Insulator-Semiconductor Optoelectronic Fibres," *Nature*, 431 826–829 (2004).
13. F. Sorin *et al.*, "Multimaterial Photodetecting Fibers: A Geometric and Structural Study," *Adv. Mater.*, 19 3872–3877 (2007).
14. A. F. Abouraddy *et al.*, "Large-Scale Optical-Field Measurements with Geometric Fibre Constructs," *Nat. Mater.*, 5 532–536 (2006).

15. M. Bayindir, A. F. Abouraddy, J. Arnold, J. D. Joannopoulos, and Y. Fink, "Thermal-Sensing Fiber Devices by Multimaterial Codrawing," *Adv. Mater.*, 18 845–849 (2006).
16. M. Bayindir *et al.*, "Integrated Fibers for Self Monitored Optical Transport," *Nat. Mater.*, 4 820–824 (2005).
17. F. Sorin *et al.*, "Exploiting Collective Effects of Multiple Optoelectronic Devices Integrated in a Single Fiber," *Nano Lett.*, 9 2630–2635 (2009).
18. S. Egusa *et al.*, "Multimaterial Piezoelectric Fibres," *Nat. Mater.*, 9 643–648 (2010).
19. N. Chocat, G. Lestoquoy, Z. Wang, D. M. Rodgers, J. D. Joannopoulos, and Y. Fink, "Piezoelectric Fibers for Conformal Acoustics," *Adv. Mater.* 39 5327–5332 (2012).
20. D. S. Deng *et al.*, "In-Fiber Semiconductor Filament Arrays," *Nano Lett.*, 8 4265–4269 (2008).
21. D. S. Deng, N. D. Orf, S. Danto, A. F. Abouraddy, J. D. Joannopoulos, and Y. Fink, "Processing and Properties of Centimeter-long, In-fiber, Crystalline-Selenium Filaments," *Appl. Phys. Lett.*, 96 023102 (2010).
22. M. Yaman *et al.*, "Arrays of Indefinitely Long Uniform Nanowires and Nanotubes," *Nat. Mater.*, 10 494–501 (2011).
23. J. J. Kaufman, G. Tao, S. Shabahang, D. S. Deng, Y. Fink, and A. F. Abouraddy, "Thermal Drawing of High-Density Macroscopic Arrays of Well-Ordered Sub-5-nm-Diameter Nanowires," *Nano Lett.*, 11 4768–4773 (2011).
24. N. D. Orf *et al.*, "Fiber draw Synthesis," *Proc. Natl Acad. Sci. USA*, 108 [12] 4743–4747 (2011).
25. S. Shabahang, J. J. Kaufman, D. S. Deng, and A. F. Abouraddy, "Observation of the Plateau-Rayleigh Capillary Instability in Multi-material Optical Fibers," *Appl. Phys. Lett.*, 99 161909 (2011).
26. J. J. Kaufman *et al.*, "Structured Spheres Generated by an In-Fibre Fluid Instability," *Nature*, 487 463–467 (2012).
27. M. Bayindir *et al.*, "Kilometer-Long Ordered Nanophotonic Devices by Preform-to-Fiber Fabrication," *IEEE J. Sel. Top. Quant.*, 12 [6] 1202–1213 (2006).
28. M. R. Lee, R. D. Eckert, K. Forberich, G. Dennler, C. J. Brabec, and R. A. Gaudiana, "Solar Power Wires Based on Organic Photovoltaic Materials," *Science*, 324 232–235 (2009).
29. P. J. A. Sazio *et al.*, "Microstructured Optical Fibers as High-Pressure Microfluidic Reactors," *Science*, 311 1583–1586 (2006).
30. T. Li, ed., *Optical Fiber Communications: Fiber Fabrication*, Academic Press, Waltham, MA, 1985.
31. H. Tokiwa, Y. Mimura, T. Nakai, and O. Shinbori, "Fabrication of Long Single-Mode and Multimode Fluoride Glass Fibres by the Double-Crucible Technique," *Electron. Lett.*, 21 [24] 1131–1132 (1985).
32. G. Urbain, Y. Bottinga, and P. Richet, "Viscosity of Liquid Silica, Silicates and Alumino-Silicates," *Geochim. Cosmochim. Acta*, 46 1061–1072 (1982).
33. K. Kakimoto, M. Eguchi, H. Watanabe, and T. Hibiya, "Natural and Forced Convection of Molten Silicon during Czochralski Single Crystal Growth," *J. Cryst. Growth*, 94 [2] 412–420 (1989).
34. D. Ofte, "The Viscosities of Liquid Uranium, Gold and Lead," *J. Nucl. Mater.*, 22 [1] 28–32 (1967).
35. A. Napolitano and E. G. Hawkins, "Viscosity of a Standard Soda-lime-silica Glass," *J. Res. Nat. Bur. Stand. Sec. A: Phys. Ch.*, 68A [5] 439–448 (1964).
36. M. Braglia *et al.*, "Rheology of Fluoride Glasses," *J. Crystal. Solid*, 213–214 [12] 325–329 (1997).
37. A. Belwalkar, W. Z. Misiolek, and J. Toulouse, "Viscosity Study of the Optical Tellurite Glass: $75TeO_2$-20ZnO-$5Na_2O$," *J. Non-Cryst. Solid*, 356 [1] 1354–1358 (2010).
38. A. S. Tverjanovich, "Temperature Dependence of the Viscosity of Chalcogenide Glass-Forming Melts," *Glass Phys. Chem.*, 29 [6] 532–536 (2003).
39. B. Chu and K. Linliu, "Viscosity Characterization of Poly(tetrafluoroethylene) by Centrifuge Ball Viscosimetry," *Macromolecules*, 28 [8] 2723–2727 (1995).
40. B. Collins, J. Shields, K. Butler, M. Seck, and T. J. Ohlemiller, "Exploring the Role of Polymer Melt Viscosity in Melt Flow and Flammability Behavior," National Inst. of Standards and Technology (BFRL), Gaithersburg, MD., ProductType: Technical report, NTIS Order Number: PB2007-105069, p 29 (2000).
41. P. Koštál and J. Málek, "Viscosity of Selenium Melt," *J. Non Cryst. Solids*, 356 [50–51] 2803–2806 (2010).
42. V. M. Glazov, S. N. Chizhevskaya, and N. N. Glagoleva, *Liquid Semiconductors*, Plenum Press, New York, 1969.
43. Y. Sato, T. Nishizuka, T. Takamizawa, T. Yamamura, and Y. Waseda, "Viscosity of Molten GaSb and InSb," *Int. J. Thermophys.*, 23 235–243 (2002).
44. M. F. Culpin, "The Viscosity of Liquid Indium and Liquid Tin," *Proc. Phys. Soc. B*, 70 [11] 1069–1078 (1957).
45. A. Dargys and J. Kundrotas, *Handbook on Physical Properties of Ge, Si, GaAs and InP*, The Science and Encyclopaedia Publishing Centre, Vilnius, 1994.
46. http://www.owlnet.rice.edu/~msci301/ThermalExpansion.pdf
47. ASM Handbook, *Properties and Selection: Nonferrous Alloys and Special-Purpose Materials (ASM Handbook)*, Vol. 2, 10th edition, ASM International, Metals Park, OH, 1990, 704-705 (Au), 1154–1156 (Si).
48. http://www.engineersedge.com/properties_of_metals.htm
49. F. C. Nix and D. MacNair, "The Thermal Expansion of Pure Metals: Copper, Gold, Aluminum, Nickel, and Iron," *Phys. Rev.*, 60 597–605 (1941).
50. http://www.ioffe.ru/SVA/NSM/Semicond/InSb/thermal.html
51. D. F. Gibbons, "Thermal Expansion of Some Crystals with the Diamond Structure," *Phys. Rev.*, 112 136–140 (1958).
52. http://www2.dupont.com/Teflon_Industrial/en_US/tech_info/tech-info_compare.html
53. M. J. Weber, *Optics Handbook of Optical Materials*, CRC Press, Boca Raton, FL, 2003, section 3.4 (Teflon-PTFE), section 2.4 (fused silica), section 2.2.4 (BK7) and section 2.5.1 (ZBLAN).
54. M. Bass, E. W. Van Stryland, D. R. Williams, and W. L. Wolfe, *Handbook of Optics Volume II Devices, Measurements, and Properties*, 2nd edition, McGraw-Hill Inc., New York, 1995, p 33.55 (fused Silica and ZBLAN) p 7.9 (Polycarbonate).
55. http://www.amorphousmaterials.com
56. http://www.polymerprocessing.com/polymers/PC.html
57. J. Ballato *et al.*, "Silicon Optical Fiber," *Opt. Express*, 16 [23] 18675–18683 (2008).
58. B. L. Scott, K. Wang, and G. Pickrell, "Fabrication of n-Type Silicon Optical Fiber," *IEEE Photon. Technol. Lett.*, 21 [24] 1798–1800 (2009).
59. H. K. Tyagi *et al.*, "Plasmon Resonances on Gold Nanowires Directly Drawn in a Step-index Fiber," *Opt. Lett.*, 35 [15] 2573–2575 (2010).
60. D. J. Gibson and J. A. Harrington, "Extrusion of Hollow Waveguide Preforms with a One-dimensional Photonic Bandgap Structure," *J. Appl. Phys.*, 95 [8] 3895–3900 (2004).
61. X. Feng, T. M. Monro, P. Petropoulos, V. Finazzi, and D. J. Richardson, "Extruded Single-mode High-index-core One-dimensional Microstructured Optical Fiber with High index-contrast for Highly Nonlinear Optical Devices," *Appl. Phys. Lett.*, 87 [8] 081110 (2005).
62. G. Tao, S. Shabahang, E.-H. Banaei, J. J. Kaufman, and A. F. Abouraddy, "Multimaterial Preform Coextrusion for Robust Chalcogenide Optical Fibers and Tapers," *Opt. Lett.*, 37 [13] 2751–2753 (2012).
63. M. Liao *et al.*, "Fabrication and Characterization of a Chalcogenide-tellurite Composite Microstructure Fiber with High Nonlinearity," *Opt. Express*, 17 [24] 21608–21614 (2009).
64. E. Snitzer and R. Tumminelli, "SiO_2-clad Fibers with Selectively Volatilized Soft-glass Cores," *Opt. Lett.*, 14 [14] 757–759 (1989).
65. H. L. Blackmore, *A Dictionary of London Gunmakers*, Phaidon-Christie's Limited, Oxford, U.K., 1986, p. 59.
66. E. Roeder, "Extrusion of Glass," *J. Non-Cryst. Solids*, 5 [5] 377–388 (1971).
67. E. Roeder, "Flow behaviour of glass during extrusion," *J. Non-Cryst. Solids*, 7 [2] 203–220 (1972).
68. W. Egel-Hess and E. Roeder, "Extrusion of Glass Melts-influence of Wall Friction Effects on the Die Swell Phenomenon," *Glasstech. Ber.*, 62 [8] 279–284 (1989).
69. P. Kaiser and H. W. Astle, "Low-Loss Single-Material Fibers Made From Pure Fused Silica," *AT&T Tech. J.*, 53 [6] 1021–1039 (1974).
70. B. Temelkuran, S. D. Hart, G. Benoit, J. D. Joannopoulos, and Y. Fink, "Wavelength-scalable Hollow Optical Fibres with Large Photonic Bandgaps for CO_2 Laser Transmission," *Nature*, 420 650–653 (2002).

71. K. Kuriki *et al.*, "Hollow Multilayer Photonic Bandgap Fibers for NIR Applications," *Opt. Express*, 12 [8] 1510–1517 (2004).
72. Z. Ruff, D. Shemuly, X. Peng, O. Shapira, Z. Wang, and Y. Fink, "Polymer-composite Fibers for Transmitting High Peak Power Pulses at 1.55 microns," *Opt. Express*, 18 [15] 15697–15703 (2010).
73. D. Shemuly, A. M. Stolyarov, Z. M. Ruff, L. Wei, Y. Fink, and O. Shapira, "Preparation and Transmission of Low-loss Azimuthally Polarized Pure Single Mode in Multimode Photonic Band Gap Fibers," *Opt. Express*, 20 [6] 6029–6035 (2012).
74. A. M. Stolyarov *et al.*, "Enhanced Chemiluminescent Detection Scheme for Trace Vapor Sensing in Pneumatically-Tuned Hollow Core Photonic Bandgap Fibers," *Opt. Express*, 20 [11] 12407–12415 (2012).
75. A. M. Stolyarov, L. Wei, F. Sorin, G. Lestoquoy, J. D. Joannopoulos, and Y. Fink, "Fabrication and Characterization of Fibers with Built-in Liquid Crystal Channels and Electrodes for Transverse Incident-Light Modulation," *Appl. Phys. Lett.*, 101 011108 (2012).
76. A. M. Stolyarov *et al.*, "Microfluidic Directional Emission Control of an Azimuthally Polarized Radial Fibre Laser," *Nat. Photonics*, 4 229–233 (2012).
77. J. N. Winn, Y. Fink, S. Fan, and J. D. Joannopoulos, "Omnidirectional Reflection from a One-Dimensional Photonic Crystal," *Opt. Lett.*, 23 1573–1575 (1998).
78. Y. Fink *et al.*, "A Dielectric Omnidirectional Reflector," *Science*, 282 1679–1682 (1998).
79. Y. Fink, D. J. Ripin, S. Fan, C. Chen, J. D. Joannopoulos, and E. L. Thomas, "Guiding Optical Light in Air Using an All-Dielectric Structure," *J. Lightwave Technol.*, 17 [11] 2039–2041 (1999).
80. P. Yeh, A. Yariv, and E. Marom, "Theory of Bragg Fiber," *J. Opt. Soc. Am.*, 68 1196–1201 (1978).
81. S. Johnson *et al.*, "Low-loss Asymptotically Single-mode Propagation in Large-core OmniGuide Fibers," *Opt. Express*, 9 [13] 748–779 (2001).
82. M. Ibanescu, S. G. Johnson, M. Soljacic, J. D. Joannopoulos, and Y. Fink, "Analysis of Mode Structure in Hollow Dielectric Waveguide Fibers," *Phys. Rev. E*, 67 046608 (2003).
83. O. Shapira, A. F. Abouraddy, J. D. Joannopoulos, and Y. Fink, "Complete Modal Decomposition for Optical Waveguides," *Phys. Rev. Lett.*, 94 143902 (2005).
84. O. Shapira, A. F. Abouraddy, Q. Hu, D. Shemuly, J. D. Joannopoulos, and Y. Fink, "Enabling Coherent Superpositions of iso-frequency Optical States in Multimode Fibers," *Opt. Express*, 18 [12] 12622–12629 (2010).
85. D. Shemuly *et al.*, "Asymmetric Wave Propagation in Planar Chiral Fibers," in preparation, 2012.
86. http://www.omni-guide.com/
87. A. Yildirim, M. Vural, M. Yaman, and M. Bayindir, "Bioinspired Optoelectronic Nose with Nanostructured Wavelength-Scalable Hollow-Core Infrared Fibers," *Adv. Mater.*, 23 1263–1267 (2011).
88. H. Qu and M. Skorobogatiya, "Liquid-core Low-refractive-index-contrast Bragg Fiber Sensor," *Appl. Phys. Lett.*, 98 201114 (2011).
89. K. J. Rowland, S. Afshar, A. Stolyarov, Y. Fink, and T. M. Monro, "Bragg Waveguides with Low-Index Liquid Cores," *Opt. Express*, 20 [1] 48–62 (2012).
90. O. Shapira *et al.*, "Surface-emitting Fiber Lasers," *Opt. Express*, 14 [9] 3929–3935 (2006).
91. S. D. Hart, G. R. Maskaly, B. Temelkuran, P. H. Prideaux, and J. D. Joannopoulos, "External Reflection from Omnidirectional Dielectric Mirror Fibers," *Science*, 296 510–513 (2002).
92. G. Benoit, S. D. Hart, B. Temelkuran, J. D. Joannopoulos, and Y. Fink, "Static and Dynamic Properties of Optical Microcavities in Photonic Bandgap Yarns," *Adv. Mater.*, 15 [24] 2053–2056 (2003).
93. G. Benoit, K. Kuriki, J. F. Viens, J. D. Joannopoulos, and Y. Fink, "Dynamic All-optical Tuning of Transverse Resonant Cavity Modes in Photonic Bandgap Fibers," *Opt. Lett.*, 30 [13] 1620–1622 (2005).
94. G. Delaizir *et al.*, "Influence of Ageing Conditions on the Mechanical Properties of Te-As-Se Fibers," *J. Phys. D*, 42 095405 (2009).
95. S. Shabahang *et al.*, "Octave-spanning Infrared Supercontinuum Generation in Robust Chalcogenide Fiber Nano-tapers using Picosecond Pulses," *Opt. Lett.* 37 4639–4641 (2012), in press.
96. M. Poulain, M. Poulain, and J. Lucas, "Verres Fluores Au Tetrafluorure de Zirconium Proprietes Pptiques d'un verre Dope au Nd^{3+}," *Mater. Res. Bull.*, 10 [4] 243–246 (1975).
97. S. A. Ray Hilton, *Chalcogenide Glasses for Infrared Optics*, McGraw-Hill, New York, 2009.
98. T. Kanamori, Y. Terunuma, S. Takahashi, and T. Miyashita, "Chalcogenide Glass Fibers for Mid-Infrared Transmission," *J. Lightwave Technol.*, 2 [5] 607–613 (1984).
99. S. Shibata and T. Manabe, "Teflon FEP-clad Fluoride Glass Fiber," *Electron. Lett.*, 17 [3] 128–129 (1981).
100. M. Saito, M. Takizawa, S. Sakuragi, and F. Tanei, "Infrared Image Guide with Bundled As-S Glass Fibers," *Appl. Opt.*, 24 2304–2308 (1985).
101. M. Saito and M. Takizawa, "Teflon-clad As-S glass Infrared Fiber with Low-absorption Loss," *J. Appl. Phys.*, 59 1450–1452 (1985).
102. J. Nishii, T. Yamashita, T. Yamagishi, C. Tanaka, and H. Sone, "Coherent Infrared Fiber Image Bundle," *Appl. Phys. Lett.*, 59 2639–2641 (1991).
103. H. Suto, "Chalcogenide Fiber Bundle for 3D Spectroscopy," *Infrared Phys. Technol.*, 38 [2] 93–99 (1997).
104. J. S. Sanghera, V. Q. Nguyen, P. C. Pureza, R. E. Miklos, F. H. Kung, and I. D. Aggarwal, "Fabrication of Long Lengths of Low-loss IR Transmitting $As_{40}S_{(60-x)}Se_x$ Glass Fiber," *J. Lightwave Technol.*, 14 [5] 743–748 (1996).
105. C. Chaudhari, M. Liao, T. Suzuki, and Y. Ohishi, "Chalcogenide Core Tellurite Cladding Composite Microstructured Fiber for Nonlinear Applications," *J. Lightwave Technol.*, 30 [13] 2069–2076 (2012).
106. M. Liao, X. Yan, G. Qin, C. Chaudhari, T. Suzuki, and Y. Ohishi, "Controlling the Chromatic Dispersion of Soft Glass Highly Nonlinear Fiber Through Complex Microstructure," *J. Non Cryst. Solids*, 356 [44–49] 2613–2617 (2010).
107. F. Luan *et al.*, "All-solid Photonic Bandgap Fiber," *Opt. Lett.*, 29 2369–2371 (2004).
108. F. Sorin, G. Lestoquoy, S. Danto, J. D. Joannopoulos, and Y. Fink, "Resolving Optical Illumination Distributions Along an Axially Symmetric Photodetecting Fiber," *Opt. Express*, 18 [23] 24264–24275 (2010).
109. A. Gumennik *et al.*, "All-in-fiber chemical sensing," *Adv. Mater.* (2012), adma201203053 (in press).
110. S. Danto *et al.*, "Fiber Field-effect Device via In-situ Channel Crystallization," *Adv. Mater.*, 22 4162–4166 (2010).
111. S. Danto, Z. Ruff, Z. Wang, J. D. Joannopoulos, and Y. Fink, "Ovonic Memory Switching in Multimaterial Fibers," *Adv. Funct. Mater.*, 21 [6] 1095–1101 (2011).
112. R. M. Wood, S. K. Sharam, and P. Waite, "Variation of Laser Induced Damage Threshold with Laser Pulse Repetition Frequency," *Laser Induced Damage in Optical Material: 1982*, eds., H. E. Bennett, A. H. Guenther, D. Milam and B. E. Newnam, Proceedings of a symposium sponsored by National Bureau of Standards, Boulder, CO, 44–49, 1984.
113. B. M. Cowan, "Optical Damage Threshold of Silicon for Ultrafast Infrared Pulses," *Laser-Induced Damage in Optical Materials: 2007*, eds., G. J. Exarhos, A. H. Guenther, K. L. Lewis, D. Ristau, M. J. Soileau and C. J. Stolz, Proceedings of the SPIE, 6720, 67201M, 2008.
114. B. Jalali, V. Raghunathan, D. Dimitropoulos, and O. Boyraz, "Raman-based Silicon Photonics," *IEEE J. Sel. Top. Quantum Electron.*, 12 [3] 412–421 (2006).
115. V. Raghunathan, D. Borlaug, R. Rice, and B. Jalali, "Demonstration of a Mid-infrared Silicon Raman Amplifier," *Opt. Express*, 15 14355–14362 (2007).
116. M. Lipson, "Guiding, Modulating, and Emitting Light on Silicon – Challenges and Opportunities," *J. Lightwave Technol.*, 23 [12] 4222–4238 (2005).
117. G. T. Reed and A. P. Knights, *Silicon Photonics: An Introduction*, John wiley & Sons, Ltd., Chichester, U.K., 2004.
118. J. Leuthold, C. Koos, and W. Freude, "Nonlinear Silicon Photonics," *Nat. Photonics*, 4 535–544 (2010).
119. J. Michel, J. Liu, and L. C. Kimerling, "High-performance Ge-on-Si Photodetectors," *Nat. Photonics*, 4 527–534 (2010).
120. J. Ballato *et al.*, "Glass-clad Single-crystal Germanium Optical Fiber," *Opt. Express*, 17 [10] 8029–8035 (2009).
121. C. McMillen *et al.*, "On Crystallographic Orientation in Crystal Core Optical Fibers," *Opt. Mater.*, 32 [9] 862–867 (2010).
122. J. Ballato *et al.*, "Binary III–V Core Semiconductor Optical Fiber," *Opt. Express*, 18 [5] 4972–4979 (2009).
123. J. Ballato *et al.*, "On the Fabrication of All-glass Optical Fibers from Crystals," *J. Appl. Phys.*, 105 053110 (2009).

124. S. Morris *et al.*, "The Influence of Core Geometry on the Crystallography of Silicon Optical Fiber," *J. Cryst. Growth*, 352 [1] 53–58 (2011).
125. N. Gupta *et al.*, "Annealing of Silicon Optical Fibers," *J. Appl. Phys.*, 110 093107 (2011).
126. J. Ballato *et al.*, "Reactive Molten Core Fabrication of Glass-clad Amorphous and Crystalline Oxide Optical Fibers," *Opt. Mater. Express*, 2 [2] 153–160 (2012).
127. S. Morris *et al.*, "Reactive Molten Core Fabrication of Silicon Optical Fiber," *Opt. Mater. Express*, 1 [6] 1141–1149 (2011).
128. S. Radic, "Parametric Amplification and Processing in Optical Fibers," *Laser Photon. Rev.*, 2 [6] 498–513 (2008).
129. P. J. Roberts *et al.*, "Ultimate Low Loss of Hollow-core Photonic Crystal Fibres," *Opt. Express*, 13 [1] 236–244 (2005).
130. D. S. Deng, J.-C. Nave, X. Liang, S. G. Johnson, and Y. Fink, "Exploration of In-fiber Nanostructures from Capillary Instability," *Opt. Express*, 19 [17] 16273–16290 (2011).
131. S. Tomotika, "On the Instability of a Cylindrical Thread of a Viscous Liquid Surrounded by Another Viscous Fluid," *Proc. R. Soc. Lond. A*, 150 322–337 (1935).
132. T. Khudiyev, E. Ozgur, M. Yaman, and M. Bayindir, "Structural Coloring in Large Scale Core-Shell Nanowires," *Nano Lett.*, 11 4661–4665 (2011).
133. A. Gumennik *et al.*, "Silicon Nanosphere Fabrication by Controlled Capillary Instability" in preparation, 2012.
134. B. R. Jackson, P. J. A. Sazio, and J. V. Badding, "Single-Crystal Semiconductor Wires Intetrated into Microstructured Optical Fibers," *Adv. Mater.*, 20 1135–1140 (2008).
135. J. R. Sparks *et al.*, "Zinc Selenide Optical Fibers," *Adv. Mater.*, 23 1647–1651 (2011).
136. D. M. Dobkin and M. K. Zuraw, ed., *Principles of Chemical Vapor Deposition*, Kluwer, Dordrecht, The Netherlands, 2003.
137. R. He *et al.*, "Integration of Gigahertz-bandwidth Semiconductor Devices Inside Microstructured Optical Fibres," *Nat. Photonics*, 6 174–179 (2012).
138. D.-J. Won *et al.*, "All-optical Modulation of Laser Light in Amorphous Silicon-filled Microstructured Optical Fibers," *Appl. Phys. Lett.*, 91 161112 (2007).
139. C. E. Finlayson, A. Amezcua-Correa, P. J. A. Sazio, N. F. Baril, and J. V. Badding, "Electrical and Raman Characterization of Silicon and Germanium-filled Microstructed Optical Fibers," *Appl. Phys. Lett.*, 90 132110 (2007).
140. A. Tuniz *et al.*, "Drawn Metamaterials with Plasmonic Response at Terahertz Frequencies," *Appl. Phys. Lett.*, 96 191101 (2010).
141. E. J. Smith, Z. Liu, Y. Mei, and O. G. Schmidt, "Combined Surface Plasmon and Classical Waveguiding through Metamaterial Fiber Design," *Nano Lett.*, 10 1–5 (2010).
142. A. Wang *et al.*, "Fiber Metamaterials with Negative Magnetic Permeability in the Terahertz," *Opt. Mater. Express*, 1 [1] 115–120 (2011).
143. A. Tuniz *et al.*, "Stacked-and-drawn Metamaterials with Magnetic Resonances in the Terahertz Range," *Opt. Express*, 19 [17] 16480–16490 (2011).
144. A. Tuniz *et al.*, "Spatial Dispersion in Three-dimensional Drawn Magnetic Metamaterials," *Opt. Express*, 20 [11] 11924–11935 (2012).
145. R. C. McPhedran, I. V. Shadrivov, B. T. Kuhlmey, and Y. S. Kivsha, "Metamaterials and Metaoptics," *NPG Asia Mater.*, 3 100–108 (2011).
146. N. Granzow, S. P. Stark, M. A. Schmidt, A. S. Tverjanovich, L. Wondraczek, and P. St. J. Russell, "Supercontinuum Generation in Chalcogenide-silica Step-index Fibers," *Opt. Express*, 19 [21] 21003–21010 (2011).
147. H. K. Tyagi *et al.*, "Plasmon Resonances on Gold Nanowires Directly Drawn in a Step-index Fiber," *Opt. Lett.*, 35 [15] 2573–2575 (2010).
148. J. Hou, D. Bird, A. George, S. Maier, B. T. Kuhlmey, and J. C. Knight, "Metallic Mode Confinement in Microstructured Fibres," *Opt. Express*, 16 [9] 5983–5990 (2008).
149. C. G. Poulton, M. A. Schmidt, G. J. Pearce, G. Kakarantzas, and P. St. J. Russell, "Numerical Study of Guided Modes in Arrays of Metallic Nanowires," *Opt. Lett.*, 32 [12] 1647–1649 (2007).
150. M. A. Schmidt, L. N. P. Sempere, H. K. Tyagi, C. G. Poulton, and P. St. J. Russell, "Waveguiding and Plasmon Resonances in Two-dimensional Photonic Lattices of Gold and Silver Nanowires," *Phys. Rev. B*, 77 033417 (2008).
151. H. W. Lee, M. A. Schmidt, H. K. Tyagi, L. N. Prill Sempere, and P. St. J. Russell, "Polarization-Dependent Coupling to Plasmon Modes on Submicron Gold Wire in Photonic Crystal Fiber," *Appl. Phys. Lett.*, 93 [11] 111102 (2008).
152. H. W. Lee *et al.*, "Pressure-assisted Melt-filling and Optical Characterization of Au Nano-wires in Microstructured Fibers," *Opt. Express*, 19 (13) 12180–12189 (2011).
153. N. Granzow, P. Uebel, M. A. Schmidt, A. S. Tverjanovich, L. Wondraczek, and P. St. J. Russell, "Bandgap Guidance in Hybrid Chalcogenide–silica Photonic Crystal Fibers," *Opt. Lett.*, 36 (13) 2432–2434 (2011).
154. P. Dragic, T. Hawkins, P. Foy, S. Morris, and J. Ballato, "Sapphire-Derived All-Glass Optical Fibres," *Nat. Photonics*, 6 627–633 (2012).